https://doi.org/10.1007/s11665-023-08705-8

Analysis of the Anticorrosion Performance and Antibacterial Efficacy of Ti-Based Ceramic Coatings for Biomedical Applications

Karima Boudjeda, Raid Bahi, Nasser Eddine Beliardouh, Chems Eddine Ramoul, Yasmine Benlala, Kheireddine Bouzid, Khokha Lalaoui, Nafarizal Nayan, and Corinne Nouveau

The anticorrosion and wear resistance, in addition to the biocompatibility are among the most important considerations in the selection of biomaterials for implants (prosthesis). It is toward this goal that titanium-based ceramic coatings were fabricated by a magnetron sputtering method. Surface characteristics, microstructures, anticorrosion behavior, calcium-phosphorus (Ca-P) layer ability formation, and antibacterial adhesion resistance were systematically investigated. Obtained results showed superior anticorrosion resistance in blood plasma of specimen coated with TiO_2 (the corrosion current density (I_{corr}) = 0.02 μA/cm^2) when compared to the specimen coated with TiN (I_{corr} = 0.81 μA/cm^2). Moreover, the in vitro bioactivity test results carried out in Hank's solution and the anti-adhesion resistance against *Staphylococcus aureus* (*S. aureus*) and *Escherichia coli* (*E. coli*) bacteria, revealed a higher performance of the TiO_2 surface when compared to TiN surface. The optimum performances (i.e., 7.3 .10^3 CFU/cm^2 versus *S. aureus* and 1.13 .10^3 CFU/cm^2 versus *E. coli*) were shown for TiO_2 (O_2 = 20%) coating characterized by fine grain microstructure, high wettability angle, and low defects density.

Keywords anticorrosion resistance, bioactivity, coatings, surface characteristics

1. Introduction

In orthopedic implant manufacture, the biomaterial must possess the following properties: a high mechanical strength, maximum resistance against corrosion, and minimum wear products (close to zero) in association with excellent biological properties, to guarantee the health and safety of patients (Ref 1).

Surface engineering has been widely studied to realize better control of the interface biomaterial/life tissue that will enhance the desired behavior. To improve further the surface capabilities of the implant, coating deposition is the appropriate strategy among numerous surface modification techniques (Ref 2). Therefore, the choice of coating must take into account all of the needed intrinsic properties mentioned above.

The microbial infection of implants is one of the most frequent and severe complications postoperative in orthopedic surgery. Implantation of a prosthesis immediately provokes the "race for the surface" i.e., competition between pathogen microorganisms (proliferation, biofilm formation) and cells-tissue integration (osteointegration, osteogenesis, angiogenesis…) for the surface colonization of the biomaterial (Ref 1-3). Many surface modifications aimed at combating biofilm formation by creating an unfavorable environment for initial microbial adhesion are under development, up to date. The surface coating technique provides implants with antibacterial properties and thus favors the host cells to win the "race" (Ref 4). That is why the scientific research in this field is far from over.

Titanium-based alloy films such as titanium nitride (TiN) and titanium oxide (TiO_2) have been popular protective coatings on implants (Ref 5, 6). They have been used as coating materials on titanium hip and Knee total prostheses, especially for their inertness toward tissues and body fluids (anticorrosion), favorable biocompatibility, and excellent clinical response (Ref 4, 6-9). Furthermore, Ti-based alloy coatings inhibit wear and corrosion products, which caused toxic reactions with the host tissue and therefore, reduce the service life of implants. Studies conducted to increase the anticorrosion resistance against aggressive environments of Ti-based alloy thin films (Ref 10, 11) as well as the tribological performances are of practical interest for the development of structural materials and ways to improve their strength characteristics (Ref 12, 13).

Karima Boudjeda, Raid Bahi, Nasser Eddine Beliardouh, Kheireddine Bouzid, and **Khokha Lalaoui**, Laboratory of Surface Engineering (LIS), Faculty of Technology, BADJI Mokhtar-Annaba University (UBMA), BP 12, 23000 Annaba, Algeria; **Chems Eddine Ramoul**, Laboratory of Surface Engineering (LIS), Faculty of Technology, BADJI Mokhtar-Annaba University (UBMA), BP 12, 23000 Annaba, Algeria; and Research Center in Industrial Technologies (CRTI), P.O. Box 64, 16014 Cheraga, Algeria; **Yasmine Benlala**, Laboratoire Central, El Bouni Hospital, Annaba, Algeria; **Nafarizal Nayan**, Microelectronic and Nontechnology Shamsudin Research Centre (MiNT-SRC), Universiti Tun Hussein Onn Malaysia, 86400 Parit Raja, Batu Pahat, Johor, Malaysia; and **Corinne Nouveau**, Arts and Métiers Institute of Technology, LABOMAP, Universite Bourgogne Franche-Comte, HESAM Université, 71250 Cluny, France. Contact e-mails: bahi.raid@gmail.com and beliardouh_23@yahoo.fr.

Graphical Abstract

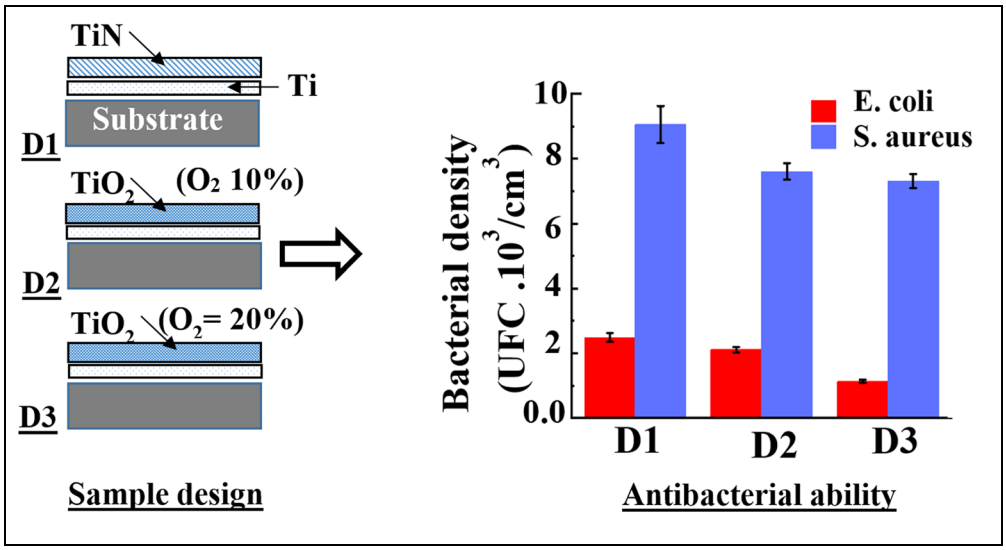

All this and other reasons (e.g., TiO_2 material possesses intrinsic antimicrobial activity due to its photocatalytic properties) make Ti-alloys more useful than others inside the human (animal) body (Ref 14, 15). However, due to its limited bioactivity, Ti-based implants have poor bio integration. Therefore, modification processes of the surface must be conducted to get the appropriate connections between the biomaterials and the bone tissue (Ref 9, 16). The production of a hydroxyapatite (HA) film on the implant surface is an effective way that enhance the osteointegration (Ref 17). HA is a major mineral component of human bones, which could provide spontaneous bonding with bone tissues and thus prevent the implant failure associated with insufficient osteointegration.

In this study, the anticorrosion resistance of titanium bioxide and titanium nitride films was investigated and compared in blood plasma as an aggressive medium. Besides, surface characteristics and the antibacterial activity were analyzed in details. The goal is to give a precise response to biomaterial manufacturers and hospital practitioners about the cost-benefit ratio of each one of them. Besides, the current trend is to develop optimized multifunctional surface coatings combining anticorrosion resistance and biocompatibility.

2. Experimental Procedures

2.1 Coatings Deposition

Titanium nitride (TiN) and titanium dioxide (TiO_2) thin films (1.5 to 2.0 ± 0.1 μm in thickness including the Ti under layer) were elaborated by a physical vapor deposition (PVD) method i.e., the reactive radio frequency (RF) magnetron sputtering using an SYNTEX/Korea system. A high purity Ti target (99.95%) was sputtered, under—600 V bias voltage and deposited upon an amorphous glass substrate (designed for corrosion and biological tests (ϕ = 10 mm x 3 mm thick)), and upon Silicon (100) wafer substrate for physical-chemical analyses (x-ray diffraction, MEB/EDS). The thickness of Si (100) is e = 370 ± 20 μm, and the Ra = 1 ± 0.2 nm. The scratch-tests are performed on specimens deposited upon titanium alloy substrates (Ti-6Al-4 V; ϕ = 20 mm x 5 mm in thickness and Ra = 0.25 ± 0.5 μm).

Before the sputtering process, substrates were ex situ ultrasonically cleaned for 10 min, in acetone and distilled water successively, and finally dried on air. After that, the substrates are etched using high-purity argon (99.99%) under 3. 10^{-3} mbar. Deposition parameters such as base pressure (9.3 .10^{-6} mbar), working pressure (6.6. 10^{-3} mbar), target-substrate distance (12 cm), and RF power (200 W) have been kept constant for all of the specimens.

Figure 1 illustrates a schematic of the design of the investigated samples. Firstly, a pure Ti layer was deposited as an adhesion layer to improve the adhesion between the coating and the substrate for 27 min in pure Ar gas (99.95%).

After that, TiN or TiO_2 layers will be deposited for 180 min in reactive gas (O_2 or N_2). During the TiO_2 coatings deposition process, two O_2/Ar ratios were used i.e., 0.11 and 0.25 for D2 and D3 samples (Fig. 1), respectively. The Ratio of N2/Ar for TiN was 0.43. The parameters of the coating's deposition, as well as the selection of the oxygen content in TiO_2 specimens, were chosen based on the previous work (Ref 18). Table 1 summarizes the main parameters used in this study.

2.2 Corrosion Testing

The electrochemical studies were carried out to investigate the anticorrosion performance using a potentiostat/galvanostat *Gamry* 600 + . A conventional three-electrode cell was used for electrochemical measurements. Tested specimens were used as the working electrodes (WE), a platinum plate as the counter electrode (CE), and a saturated calomel electrode (SCE) as a reference electrode (RE). A human blood plasma (Fresh frozen blood plasma) at pH∼7.4 was selected to be the tested medium (50 ml per test). Generally, the blood Plasma contains about 90% water, with 10% being made up of ions, proteins, dissolved gases, nutrient molecules, and wastes. The average concentration of the ionic components (in [mol/L].10^{-3}) of the blood plasma, generally given in the literature, is Na^+ = 142.0, K^+ = 5.0, Ca^{2+} = 2.5, Mg^{2+} = 1.5, Cl^- = 103.0, $(HCO_3)^-$ =

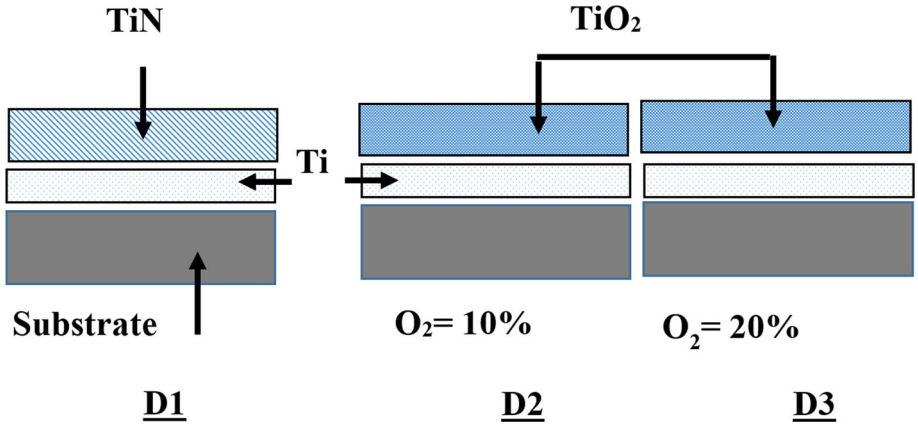

Fig. 1 Schematic of the specimen design: D1 (TiN), D2 (TiO_2 (10%)), and D3 (TiO_2 (20%))

Table 1 Coating deposition parameters

	Gas flow, sccm			Total time process, min
Specimen	Ar	N_2	O_2	
D1	70	30	…	207
D2	90	…	10	207
D3	80		20	207

27.0, HPO_4^{2-} = 1.0, $(SO_4)^{-2}$ = 0.5, and the Ca/P = 2.5 (Ref 19).

The potentiodynamic polarization test was raised from − 1 V to + 1 V, at a scan rate of 1 mV/s. Before the test, specimens were immersed in the electrolyte for 1 h to attain stable open circuit potential (OCP). The main electrochemical parameters of the working electrode are calculated based on the Tafel and polarization curves. The polarization resistance (*Rp*) was estimated from linear polarization measurements as the slope of the linear region of the ΔE-Δi curve. The corrosion potential (E_{corr}), and anodic and cathodic slopes (βa, βc) are estimated from Tafel plots. The corrosion current density (I_{corr}) is calculated based on previously determined parameters using the Stern-Geary equation (1) as follows:

$$Rp = \frac{\beta a.\beta c}{2,3039(\beta a + \beta c)} \times \frac{1}{I\text{corr}} \quad \text{(Eq 1)}$$

The electrochemical impedance spectroscopy (EIS) tests were performed after 1 h of immersion of the working electrode in the blood plasma at 37 ± 0.5 °C, during which the OCP was recorded to ensure the stability condition. The impedance data are collected within a frequency range of 100. 10^3 Hz to 10^{-2} Hz, at a rate of 5 points/decade at OCP condition with an alternating current (AC) amplitude of 10 mV. The impedance data were fitted by an electrical equivalent circuit (EEC) using *EC-Lab Software*. Each electrochemical test was performed at least three times to ensure the reproducibility of data.

2.3 Bioactivity Tests

The in vitro bioactivity of all samples deposited onto Si (100) substrates was evaluated in terms of their apatite-forming ability by soaking the samples in 20 ml of Hank's solution at 37 °C, which was renewed regularly after 24 h for 21 days. The ionic concentrations of Hank's solution compounds are nearly equal to those of human plasma ((mol/L). 10^{-3}): Na^+ = 142.0, K^+ = 5.0, Mg^{2+} = 1.0, Ca^{2+} = 2.5, Cl^- = 131.0, $(HCO_3)^-$ = 5.0, $(HPO_4)^{2-}$ = 1.0, $(SO_4)^{2-}$ = 1.0 and the pH = 7.0 − 7.4).

After exposure, the samples were extracted, washed in double-distilled water, and dried at 100 °C. The final step was SEM/EDS analyses to evaluate (qualitatively) the mineral layer formation at the top surface

2.4 In Vitro Anti-Bacterial Adhesion Tests

Gram-negative *Staphylococcus aureus* (S. *aureus*) and gram-positive *Escherichia coli* (*E. coli*) bacteria were selected to evaluate the antibacterial activity of TiN and TiO_2 coatings deposited onto a glass substrate. The first step is to place the tested specimens (D1, D2, and D3) in contact with bacteria. Beforehand, samples were sterilized within Petri dishes, using a drying oven at 100 °C for 90 min. In the meantime, a stock solution (bacterial suspension) has been prepared in a nutrient solution called "Buffered Glucose Broth (BGT)." After that, the stock solution will be poured slowly inside the Petri dishes (samples). The bacterial suspension quantities used in this study are ~8.25. 10^3 UFC/ml and ~45.0. 10^3 UFC/ml for *E. coli* and *S. aureus,* respectively (CFU means Colony Forming Unit). An incubation period of 24 h at 37 °C was kept constant for all the biological samples (Petri dishes). The second step is to wash samples in physiological solution (0.9% NaCl in aqueous solution), then vigorously cleaned with a vortex mixer to detach bacteria from the surfaces of the specimens (D1, D2, and D3). Detached bacteria were collected in new petri dishes, containing agar (nutrient) and will be maintained for a second incubation period for 24 h at 37 °C. The final step is to count the colony densities (UFC/cm^2). All biological tests were carried out in strict compliance with workspace sterilization and were repeated twice.

3. Results and Discussion

3.1 Microstructural Surface Analysis

3.1.1 X-ray Diffraction Analysis (XRD). To define the structures of the deposits made, XRD analyses were carried out by using the conventional symmetrical Bragg-Brentano con-

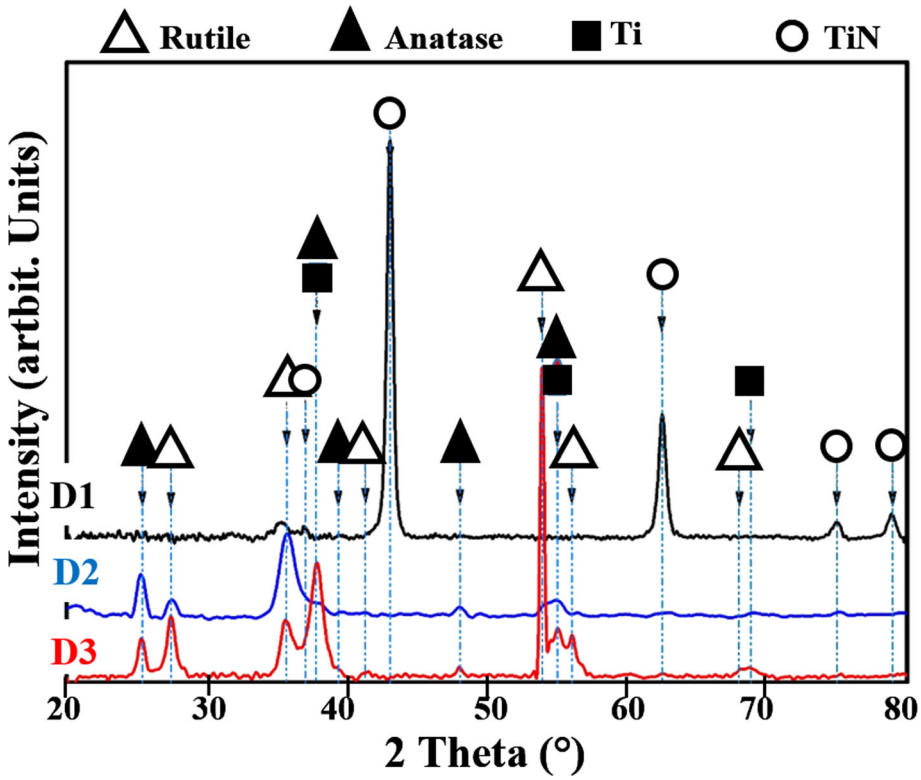

Fig. 2 The x-ray diffraction patterns spectra of the tested specimens: D1 (TiN), D2 (TiO_2 (10%)), and D3 (TiO_2 (20%))

figuration. The obtained x-ray diffractograms are shown in Fig. 2. The D1 sample indicated the presence of crystalline Ti-phase and TiN-phase, according to the standard ICDD cards (International Centre for Diffraction Data) N° 01-089-3726 and 00-031-1403, respectively. Figure 2 also indicates that the D2 and D3 samples are composed of the TiO_2 anatase phase (ICDD standard cards N° 01-073-1764) and the TiO_2 rutile phase (ICDD standard cards N° 98-003-3844).

3.1.2 Coating Adherence. The coating adherence characterizes the mechanical resistance of the interface between the coating and the substrate. The adherence tests of coated specimens were carried out using a *Millennium* 200 *Scratch Tester*, equipped with a conical diamond tip (radius = 0.2 mm), to characterize the critical load at which failure occurs in dry conditions (load increase rate = 79 N/min, sliding velocity = 8 mm/min, and the scratch length = 8 mm). Three (03) scratch experiments were conducted on each tested sample. The critical load of cohesive (L_{C1}) and adhesive damage (L_{C2}) are (L_{C1} = 6, 5 ± 0.5 N; L_{C2} = 111.48 ± 1.5 N) for D1 (TiN) specimen. Specimens D2 (TiO_2 (10%)) and D3 (TiO_2 (20%)) displayed equal values (L_{C1} = 6.7 ± 1.0 N; L_{C2} = 15.3 ± 1 N).

3.1.3 Surface Morphologies. Figure 3 shows the surface morphologies of the deposited coatings obtained by two different techniques. The SEM micrographs revealed typical columnar growth microstructures with domes i.e., the tops of the columns (Fig. 3a, c, and e). Pinholes, micro-pores, protrusions, and macroparticles (droplets) could be seen on the surfaces of both TiN and TiO_2 PVD coatings, as expected. The aspect of the columnar structure is shown in Fig. 3c, whereas an example of a defect (droplet) is presented in Fig. 3e.

Small globular grains with a narrow particle size distribution are observed in the case of D1 coating specimen (Fig. 3a). The D2 and D3 specimens exhibited denser microstructures with homogeneous grain sizes when compared to the D1 case (Fig. 3 and 3). Moreover, domes become smaller with increasing oxygen content (D3 case).

In order to obtain further information on the surface characteristics, the atomic force microscopy technique (AFM) was carried out using a *Park System XE−100/Korea*. Consequently, additional quantitative information can be obtained such as surface roughness with high accuracy, which helps to better understand the different mechanisms evolved during the electrochemical tests.

During AFM analysis, the distance between the cantilever and the substrate's surface is very close, about 10 nm, without touching (non-contact mode). The cantilever lip oscillates with a specific scan rate of 1.5 Hz over the entire scan area of the sample (1 μm^2). The sample was scanned line by line and then gathered by simulation, to obtain the surface topography. In this study, the roughness was characterized by the arithmetic average roughness (*Ra*) and the quadratic average roughness (*Rq*). Obtained results, based on statistical data processing using *Gwyddion Free Software*, are shown in Table 2.

Finally, the deposited coatings have a columnar microstructure with globular domes. It is indicated that D1 presents the highest roughness, while D3 shows a low grain size and the denser microstructure.

3.1.4 Wettability. In the field of biomaterials, the wettability (the surface free energy) has long been understood as a defining parameter in determining cellular adhesion (osteointegration) and a key factor to prevent biofilm formation (Ref 20).

The hydrophobicity of the surface is based on the evaluation (measure) of the angle value between the drop of water and the surface of the material. For this purpose, a volume of 0.2 μL of

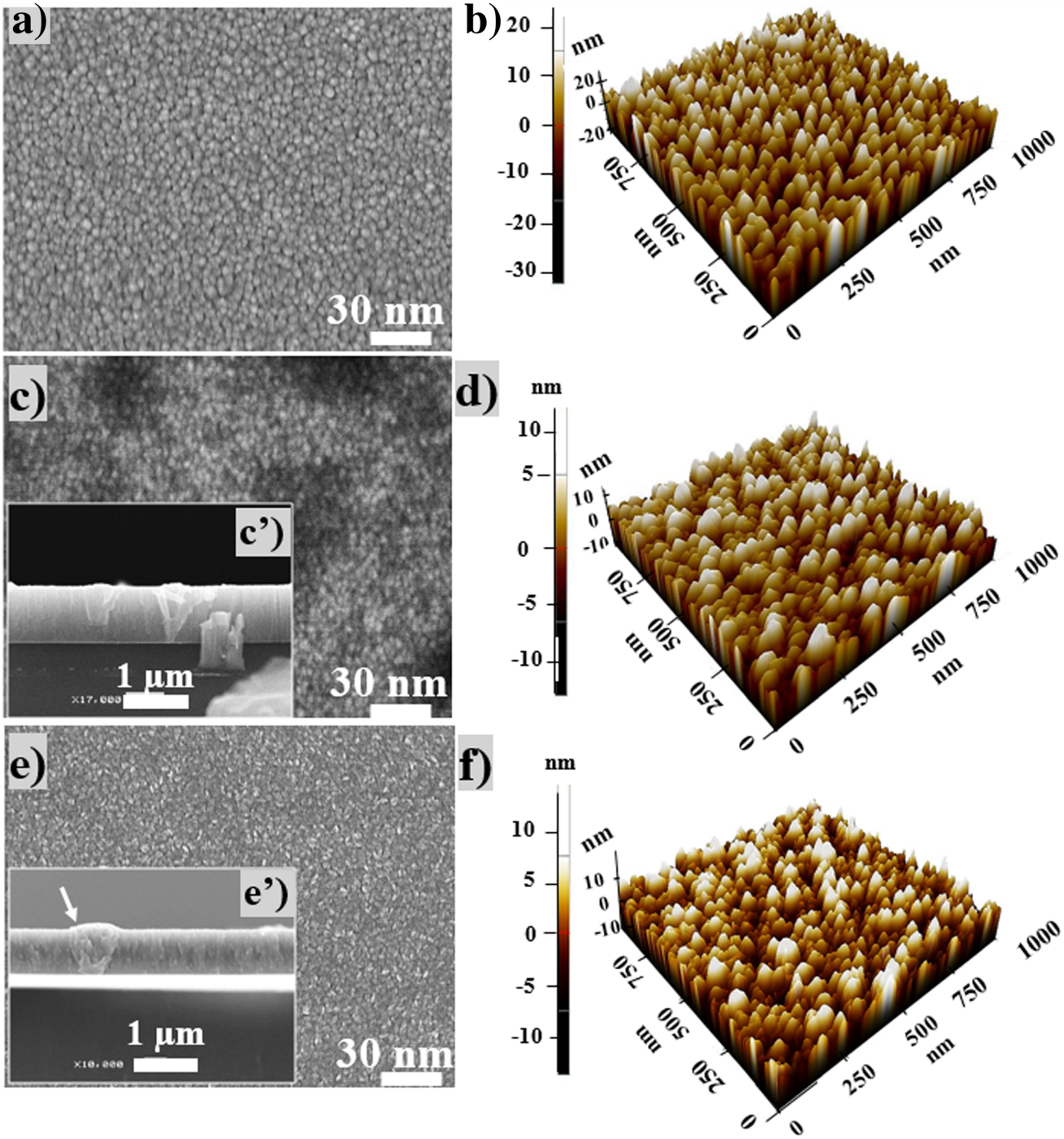

Fig. 3 SEM micrographs and AFM images from the top surfaces of the deposited coatings; (a, b): D1-(TiN), (c, d): D2 (TiO_2 (10%)), and (e, f): D3 (TiO_2 (20%)). (a') The cross-sectional view of D2 specimen and (e') cross-sectional view of D3 specimen (the white arrow shows a microstructural defect) (Color figure online)

deionized water is placed on the surface of the samples. Five drops of each liquid were recorded to determine the measurements.

Figure 4 shows the average wettability angles (θ) of each sample. As one can see, (Fig. 4a-c), the D3 specimen exhibits the highest θ value which approaches 90°. However, it must be noticed that the θ (D1) $\approx$ 72° is greater than θ (D2) (TiN versus TiO_2 (10%); this could be related to the lower electronegativity of nitride-based coatings as compared to oxide-based coatings (Ref 21). However, increasing the oxygen percentage (TiN versus TiO_2 (20%), leads to an opposite phenomenon i.e., an increase in hydrophobicity of D3. These data are consistent with the findings of contact angle measurements using the sessile drop technique on surface free energy analysis of PVD coatings of TiN and TiO_2 systems (Ref 20, 22). The authors considered that the difference observed in θ values between TiN and TiO_2 was due to the reduction in oxidation states (from Ti^{4+} to Ti^{3+}) by water (Ref 22).

Generally, when a liquid comes into contact with a surface, the resulting wettability depends on numerous factors (such as

surface roughness, surface chemistry, surface tension, and porosity, among others) of the involved solid surface (Ref 23-25). The influences of these factors on the wettability angle measurements are explained in detail in the literature (Ref 26, 27). In this study, the hydrophobicity of the D3 surface TiO_2 could come (probably) from the highest density of the surface morphology (low pores and other defects).

3.2 Corrosion Behavior

3.2.1 Potentiodynamic Polarization Curves. Figure 5 shows the potentiodynamic polarization curves of the tested specimens after 1 h of immersion (time to achieve equilibrium) in the electrolyte at 37 °C. These curves allow finding the values of the anodic and cathodic slopes, required to calculate the corrosion parameters for each specimen. A lower corrosion current density and higher corrosion potential indicate that the sample has relatively excellent corrosion resistance. As can be seen, the three curves (Fig. 5) showed the same trends in the anodic and cathodic regions, in general. Figure 5 also evidences that the TiO_2 surface has the best electrochemical behavior because it presents the lowest *I*corr in both the anodic and cathodic regions. Besides, the best resistance against corrosion is presented by the D3 sample (Fig. 5; slope in blue).

The evolution of the D3 curve (taken as an example) shows a corrosion potential of *E*corr = − 580 mV/SCE. From this value up to approximately a potential of zero (0.0) mV/SCE, the curve indicates a well-defined linear range in the anodic region, that corresponds to the self-passivation domain. The existence of this passive region is due to the spontaneous formation of a thin oxide (passive layer) on the external surface. From 0.0 up to + 0.35 mV/SCE, the current density increases indicating a breaking dawn of the passive film i.e., the dissolution of the passive film took place (corrosion). Beyond 0.35 mV/SCE, a second passivation region started again until the end of the tested potential range. The quantitative values of the corrosion parameters are reported in Table 3. Although the anti-corrosion property of TiN coating was attributed to its stable electronic structure brought about by strong interactions between Ti 3d and N 2p orbitals (Ref 28), it is clear that, in the conditions used in this study, the TiN surface has the lowest performances than that for other samples.

Compared to the TiN surface, the high electrochemical performance of the TiO_2 surface may be due to its superior hydrophobicity. Indeed, it was demonstrated that the resistance of the TiO_2 surface to corrosion current increased due to the low surface free energy (Ref 29). Furthermore, the protective TiO_2 film has low electrical conductivity and can behave like a barrier for electron transportation, as reported by Tekdir et al. (Ref 30).

3.2.2 Electrochemical Impedance Spectroscopy. Figure 6 shows the results of the EIS analysis. Nyquist plots (Fig. 6a) and Bode plots (Fig. 6b) are selected to investigate the electrochemical performance of the specimens. Nyquist plots in Fig. 6a show that all samples have arcs (large incomplete semicircles) with different radii of curvature. It has been well demonstrated that increasing the diameter of the semicircle is an indication of higher corrosion resistance. Therefore, Fig. 6a indicates that the D3 specimen has the largest one. Moreover, all Nyquist plots reveal two (02) capacitive loops; the first one

Table 2 Surface roughness and grain size of the tested specimens

Specimen	Roughness, nm		Grain size, nm
	Rq	Ra	
D1	7,741 ± 0.02	6,199 ± 0.01	38 ± 5
D2	3,281 ± 0.03	2,623 ± 0.03	29 ± 3
D3	3,83 ± 0.03	2,053 ± 0.03	20 ± 2

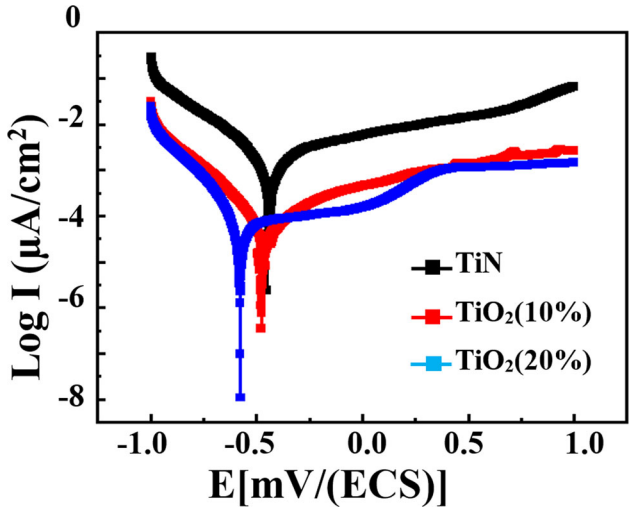

Fig. 5 Potentiodynamic curves of the investigated systems: D1 (TiN), D2 (TiO_2 (10%)), and D3 (TiO_2 (20%))

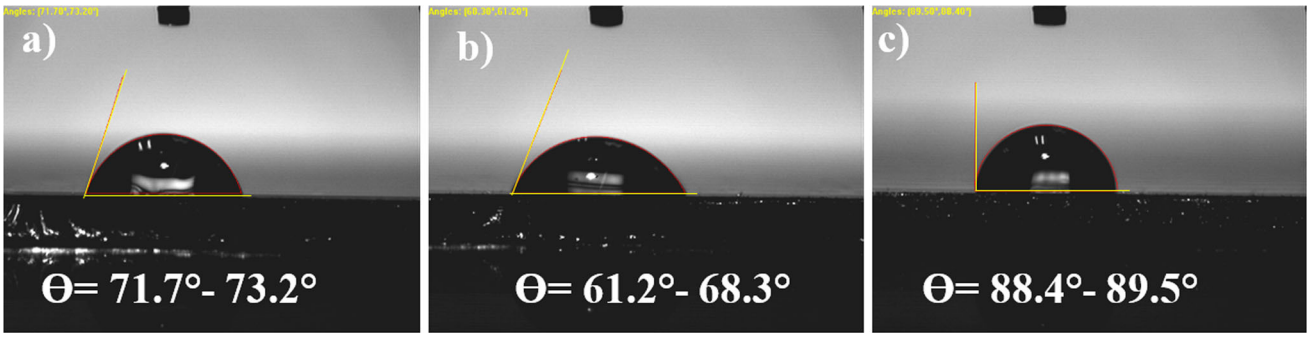

Fig. 4 Water contact angles for the tested specimens: (a) D1 (TiN), (b) D2 (TiO_2 (10%)), and (c) D3 (TiO_2 (20%))

Table 3 Potentiodynamic polarization parameters of different coatings in Blood Plasma at 37 °C

Samples	E_{corr}, mV	I_{corr}, μA cm^{-2}	β_a, mV dec^{-1}	β_c , mv dec^{-1}	Corrosion rate, mmpy*	Rp, Ω cm^2
D1	−450.023	0.809	311.9	162.4	$0.02.10^{-2}$	56.43
D2	−480.943	0.022	205.0	65.9	$1.013.10^{-3}$	983.88
D3	−580.365	0.020	144.3	69.7	$0.774.10^{-3}$	1019.9

(*mm per year).

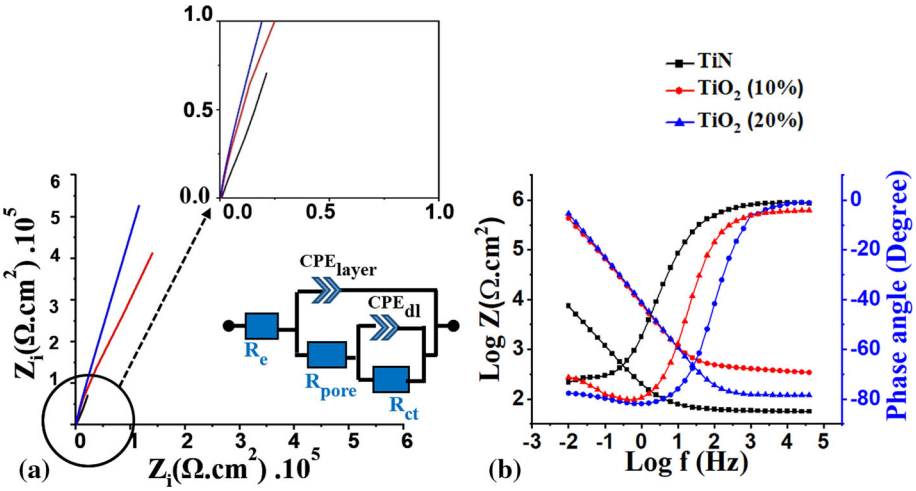

Fig. 6 Electrochemical impedance spectroscopy results (a) Nyquist plots with the chosen electrical equivalent circuit and (b) Bode plots of the investigated specimens: D1 (TiN), D2 (TiO_2 (10%)), and D3 (TiO_2 (20%))

Table 4 EIS parameters of the tested specimens in blood Plasma at 37 °C

Samples	Re, Ω cm^2	CPE_{layer} , μF/cm^2	a_1	R_{pore} , Ω cm^2	CPE_{dl} ,μF/cm^2.10^{-6}	a_2	R_{ct} ,Ω cm^2.10^3
D1	58.82	$1.252\ .10^{-3}$	0.798	2650	26.43	0.996	1.722
D2	337	$7.254\ .10^{-6}$	0.741	149.7	16.86	0.947	3.145
D3	117.7	$11.59\ .10^{-6}$	0.854	11.46	10.19	0.958	7.142

is at the high frequency, and the second one is at the medium frequency side. Besides, the capacitive character of the passive layer is clearly shown in the Bode plots (Fig. 6b). In a wide range of frequency, the impedance modulus remains a straight line, the inclinations are close to 1, and the phase angle tends to zero at the high-frequency range. The Bode diagrams also implicated two relaxation time constants, representing the rate of the electrochemical reactions.

The obtained spectra were interpreted in terms of an EEC (electrical equivalent circuit). The EEC (inset in Fig. 6a) is composed of the following circuit elements: Re represents the resistance of the electrolyte, CPE_{layer} represents the coating capacitance, (constant phase element of the barrier layer) and R_{pore} is the resistance associated with pores and the coating's defects (i.e., the current flow resistance through the pores). CPE_{dl} is the double layer capacitance in parallel with the charge transfer resistance R_{ct}. A CPE was adopted because the "a" parameter is less than 1 in both cases. The fitting data were obtained using *EC-lab software,* as summarized in Table 4. The average value of chi-square (χ^2), obtained for all of the experiments was in the order of (5 to 6). 10^{-3}. The lower value of R_{pore}, thus the greater values of R_{ct}, of the TiO_2 coatings (D2 and D3) could be attributed to the lower porosity and hence, the lower penetration of the electrolyte into the coating (Ref 31).

Summary, the observed EIS results are in a good correlation with the results obtained using the potentiodynamic polarization method. Both TiO_2 and TiN coatings are able to form a protective oxide layer. The D3 specimen exhibited superior anticorrosion resistance, which could be attributed to the lower density of defects (pores) and to the chemical stability in blood plasma environment.

3.3 In Vitro Bioactivity Analysis

One of the essential requirements for a biomaterial to bond (in vivo) to living bone is the formation of a bone-like apatite layer on its surface. It is from this perspective that bio-reactivity tests were carried out here.

Figure 7 displays the SEM micrographs of the tested specimens soaked in Hank's solution. As shown in Fig. 7a, b and c, the surfaces of the specimens are entirely covered by a calcium phosphate coating (Ca-P layer) with a "spongy

morphology." These microstructures are mainly characterized by brittleness in addition to a "hazardous growth" of mineral crystals and "heterogeneous" interconnected pores. The Ca-P layer, formed on the material's surfaces from simulated body fluid solutions (SBF) was considered as a hydroxyapatite layer (HA) or a carboxyapatite (CHA) by numerous authors, and is still very much in demand due to its chemical and crystallographic structure being similar to that of bone mineral (Ref 32).

Images in Fig. 7a, b and c show the EDS spectra of the D1, D2 and D3 coatings (spectra in yellow) as well as the EDS spectra of the corresponding Ca-P layers; which formed during the bioreactivity tests (spectra in red). The quantitative EDS

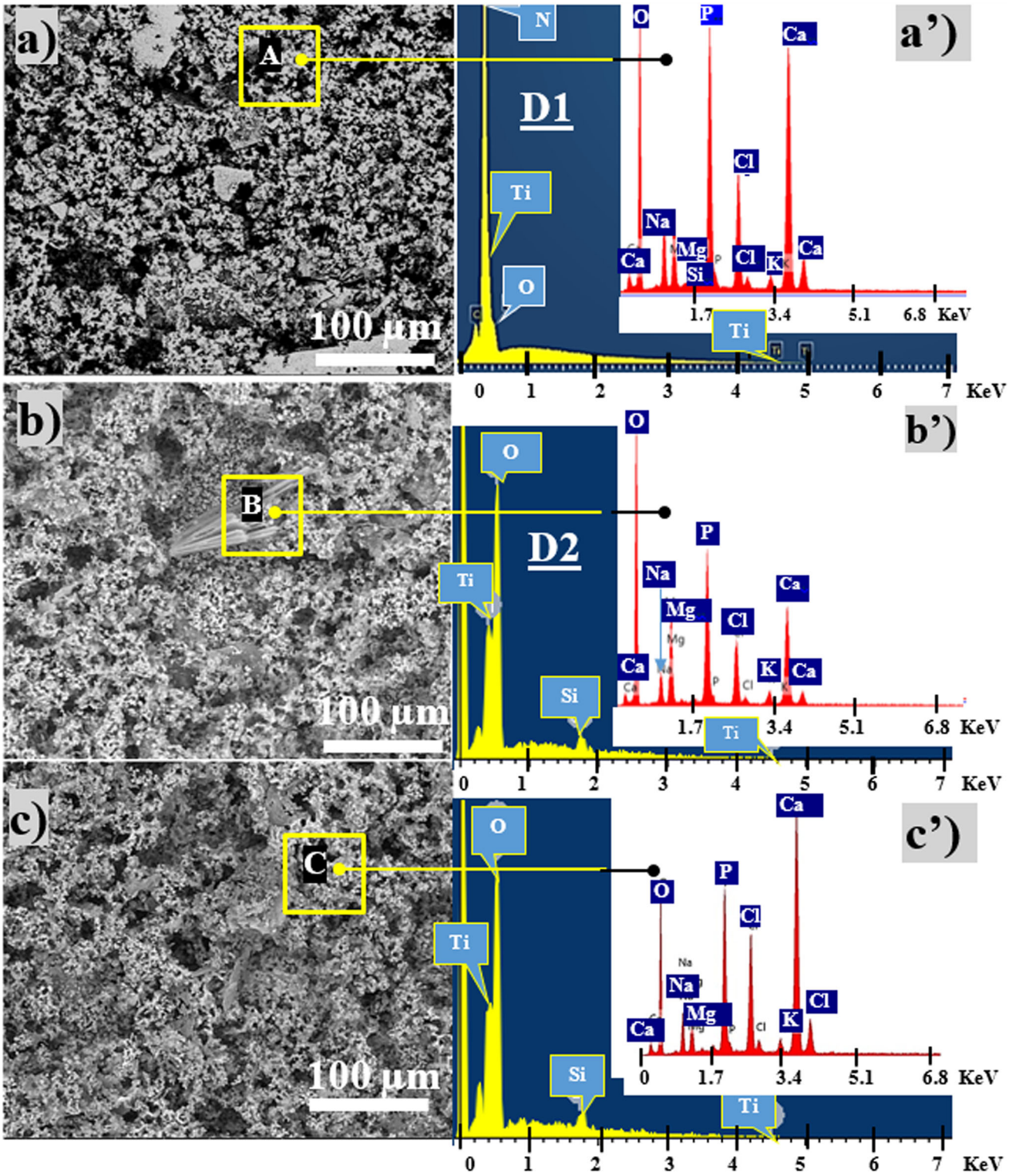

Fig. 7 SEM images of Ca-P layer formation upon surfaces of the tested specimens: (a) D1 (TiN), (b) D2 (TiO_2 (10%)), and (c) D3 (TiO_2 (20%)). (a', b', and c' EDS spectra of the coatings (in yellow) and the corresponding Ca-P layer (in red) at the indicated squares (Color figure online)

results (average values) for all tested specimens are presented in Table 5. Obtained results indicated approximately similar chemical compositions for all samples.

As presented in Table 5, the D3 sample shows a higher content of Ca than D2 and D1, whereas the contents of O and P are close enough. The average concentration ratios of Ca:P (the molar Ca/P ratio), calculated for D1, D2, and D3, are 0.89, 0.57 and 1.46, respectively. Therefore, except for D3, the semi-quantitative analysis shows that the composition of the Ca-P layers for D1 and D2 is not close to the physiological HA (Ca/P ratio in the range 1.35-1.46), nor to CHA i.e., Ca/P ratio in the range 1.33 -1.8 (Ref 32, 33).

Therefore, a better nucleation of the HA layer seems to take place on the denser surface (the D3 specimen) due to their higher degree of hydration as described in the literature (Ref 34, 35). The OH groups adsorbed on the surface substrates (TiN or TiO_2) play an important role in the nucleation process since the adsorption of Ca is supposed to initiate the nucleation of the apatite phase (Ref 36, 37). One possible explanation is the larger specific surface area of a denser surface (D3), which can carry more OH groups and therefore favors a dense formation of apatite nuclei, thus the HA formation (Ref 38).

It should be noted here that magnesium (Mg), sodium (Na), potassium (K), and chlorine (Cl) were also detected by EDS analysis (inset in Fig. 7a, b and c).

Table 5 EDS analysis results of the obtained Ca-P layers

	Elements, mass %						
Label	**O**	**Na**	**Mg**	**P**	**Cl**	**K**	**Ca**
D1	50.16	10.46	6.65	12.23	5.45	0.61	14.02
D2	48.73	8.14	5.07	10.85	4.3	0.78	7.97
D3	48.0	8.14	5.07	10.34	7.30	0.85	19.56

The cations Mg^{2+} and Na^{+} might substitute the Ca^{2+} in apatites, as reported by numerous works (Ref 33). The main reason for the existence of sharp peaks of Cl is due to the existence of Cl^{-} ions ($Cl^{-} = 131.\ 10^{-3}$ mol/L), voluntarily introduced in the initial Hank's solution (section 2.3) to reach natural conditions of the in vitro bioactive tests, because the natural apatite contains Chlorine (Ref 33-34). In fact, most biological apatites (e.g., human bones) contain a small amount of several foreign ions mainly the cations Mg^{2+}, Na + , K^{+}, and the anions $(CO_3)^{2-}$, $(HPO_4)^{2-}$, F^{-}, Cl^{-}, and they are non-stoichiometric. Additionally, Cl^{-} ions have a direct influence on the apatite-forming ability of the Ti alloy surfaces. The influence of Cl^{-} ions occurs through the surface charges (negative, positive, or neutral, as the case may be) produced by the dissociated chlorine ions and the released sodium ions, thus depending on the pH of the SBF solution as reported by Nga et al. (Ref 39).

3.4 In Vitro Antibacterial Adhesion Performance

3.4.1 Assessment of Bacterial Adhesion. Figure 8 shows aspects of the analyzed specimens (petri dishes). The bacteria colonies appeared colored in yellow with this method, and therefore, counts are easy. As described above (section 2.4), the density of the residual colonies of bacteria is estimated directly by optical microscopy.

Figure 9 displays the quantitative results of the bacterial anti-adhesion tests of the investigated surfaces versus *E. coli* and *S. aureus* bacteria. Overall, as one can see, bacterial adhesion occurred with all the materials, thus no total absence of adherence was shown.

The TiO_2 surface (D2 and/or D3) showed better performance. In other words, TiN coating surface was observed to have the lowest proclivity toward bacterial adherence. The ability for high adherence was observed with *S. aureus* in all cases.

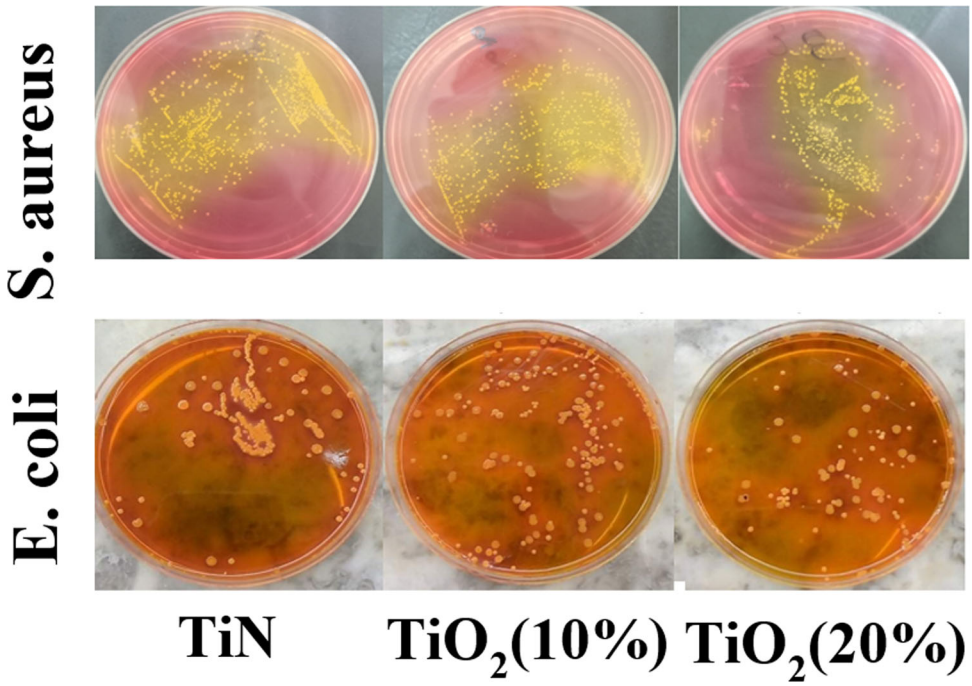

Fig. 8 Anti-bioadhesion test analysis of the investigated specimens (D1 (TiN), D2 (TiO_2 (10%)), and D3 (TiO_2 (20%)) against *E. coli* and *S. aureus* bacteria

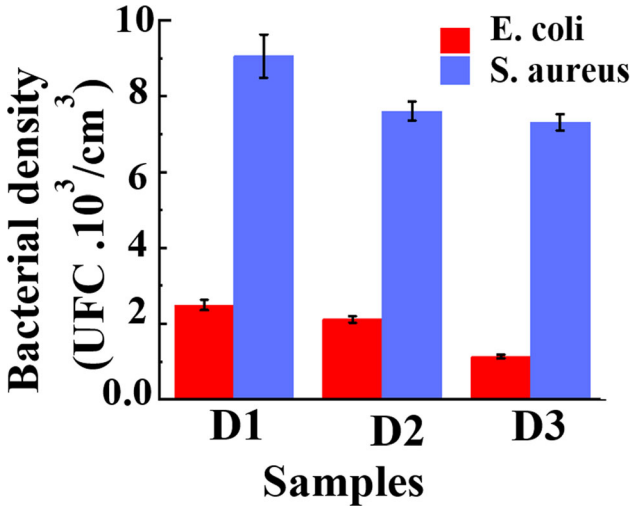

Fig. 9 Antibacterial adhesion test results of the investigated specimens: (D1 (TiN), D2 (TiO_2 (10%)), and D3 (TiO_2 (20%))

Precisely, the D3 specimen presents less residual adhered bacteria ((7.3 ± 0.22) $.10^3$ versus *S. aureus* and (1.13 ± 0.05) $.10^3$ CFU/cm^2 versus *E. coli*), whereas the D1 exhibits the worst performance ((9.2 ± 0.57) $.10^3$ and (2.49 ± 0.13) $.10^3$ CFU/cm^2 versus *S. aureus* and *E. coli*, respectively).

3.4.2 Discussion. The process of biofilm formation in *vivo* on titanium biomaterials used as implants (prostheses) is a complex of multifunctional steps. Biofilms are multicellular agglomerations of microorganisms that have catastrophic consequences for the patient's health. Pathogens anchored on the titanium surface through various surface interactions can produce biofilms. The literature suggests that the difference in bacterial adhesion ability to different material surfaces is principally due to the roughness, hydrophilicity, crystalline phase, surface topography, and surface charges which influence protein adhesion, according to the recent review by Tardelli et al. (Ref 23).

In this work, the evaluation of the adherence property of different biomaterial surfaces showed significant differences in global bacterial adhesion between TiO2 and TiN surfaces toward *E. coli* and *S. aureus* bacteria. In all cases *E. coli* presented the least adherence potential than *S. aureus*. This result is consistent with the findings of Vishwakarma et al. (Ref 22). Malhotra et al. (Ref 40) reported the same result regarding *E. coli* (weak adherence to Ti alloys), while in contrast, *S. aureus* strains showed no adhesion to the same tested biomaterials.

The main reason regarding such a great difference in the number of CFU/cm^2 value of D1, D2 and D3 surfaces against *E. coli*, and *S. aureus* bacteria can be attribute in part, to the difference in TiO_2/TiN phase microstructure. Indeed, TiO_2 microstructure possesses intrinsic antimicrobial activity against several pathogens *in vitro* due to its photocatalytic properties (Ref. 15), while no similar advantages were reported for TiN microstructure. The antimicrobial properties of TiO_2 derive from the combination of two different characteristics of these materials, namely, their self-cleaning and self-disinfection properties, as reported by Visai et al. (Ref 14). Vishwakarma et al. (Ref 22) and Del Curto et al. (Ref 41) have demonstrated that the TiO_2-anatase phase reduces bacterial adhesion and subsequent colonization on the surfaces that produce biofilms.

The second reason of the highest degree of bacterial invasion shown on TiN surface is probably the surface roughness. Although the surface roughness parameters of TiN surface can be considered moderate values (Ra∼6 nm, Rq∼7 to 8 nm), however, they exceed by more than twice the value obtained in the TiO_2 surface case (Table 2). The results obtained in this work are consistent with most of the literature data. Yoda et al. (Ref 42) demonstrated that the rough surface presents higher bacterial adhesion, as it provides a greater surface area, and the depressions in the roughened surfaces can provide more favorable sites for colonization. In contrast, Ludecke et al. (Ref 43) established that an increase in the roughness of titanium surfaces at a nanometric scale decreased the number of adhesion points, subsequently reducing adhesion of *E. coli* and *S. aureus* bacteria. Other studies have reported no correlation between roughness and bacterial adhesion ability (Ref 44).

Hydrophobicity is another factor that also governs bacterial adhesion together with surface roughness. As mentioned above (section 3.1.4) high hydrophobicity leads to weak bacterial adhesion (TiO2 (20%) specimen), thus high antibacterial performance. These results are consistent with those reported by Shah et al. (Ref. 26).

Finally, the bacterial cell surface's ability to create anchor links (e.g., secretion of specific proteins, acids, collagen) when in contact with a specific surface (Ref 45) is another way to understand the difference in the interaction between the tested material surfaces and bacteria. These are the limitations of this study, in addition to *in vivo* testing.

4. Conclusions

According to the results and within the limitations of this study, it can be concluded as follows:

- Columnar growth microstructure characterizes all of the deposited coatings.
- The electrochemical behavior of all specimens was similar, and the best electrochemical performances were displayed by the TiO_2 microstructure. Specimen labeled D3 (TiO_2 (20%) presents the lowest current density and the highest charge transfer resistance (impedance) due to its denser microstructure with less pores and defects.
- The in vitro bioactivity tests indicated that the Ca-P layer nucleation and growth were accelerated on the D3 coating, as it has the highest calculated molar Ca/P ratio (≈ 1.46) which favors a dense formation of apatite nuclei.
- The D3 coating exhibited superior anti-adhesion efficiency against S. aureus and E. coli bacteria than samples coated TiN because of their surface characteristics (wettability, roughness, defect density…).
- Tested in the same conditions, it is clear and preferable to consider titanium bi-oxide (TiO_2) with a high oxygen content as an orthopedic biomaterial.

Acknowledgments

The authors would like to thank the Ministry of Higher Education and Scientific Research of Algeria for supporting this work. The

authors are also grateful to Pr. Said BOUKHERCHE for his assistance in corrosion tests.

Author Contributions

All authors equally contributed to the study conception and the experimental activities.

Funding

The authors declare that no funds, grants, or financial supports were received during the preparation of this work.

Data Availability

The statistical data used to support the findings of this study are available from the corresponding author upon request.

Conflict of interest

The authors declare that they have no known competing financial interests or personal relationships that could have appeared to influence the work reported in this paper.

Ethical Approval

The experiments carried out in this study did not involve human tissue.

References

1. F. Batool, H. Özçelik, C. Stutz, P.Y. Gegout, N.B. Jessel, C. Petit, and O. Hunk, Modulation of Immune-Inflammatory Responses Through Surface Modifications of Biomaterials to Promote Bone Healing and Regeneration, *J. Tissue. Eng.*, 2021, **12**, p 1-19. https://doi.org/10.1177/20417314211041428
2. H. Liu, X. Zhang, S. Jin, Y. Zhao, L. Ren, and K. Yang, Effect of Copper-Doped Titanium Nitride Coating on Angiogenesis, *Mater. Lett.*, 2020, **269**, p 127634. https://doi.org/10.1016/j.matlet.2020.127634
3. C.R. Arciola, D. Campoccia, G.D. Ehrlich, Montanaro L, Biofilm-Based Implant Infections in Orthopaedics. In: Donelli, G. (eds) Biofilm-Based Healthcare-Associated Infections. *Adv Exp Med Biol*, 2015, **830**, 29-46. https://doi.org/10.1007/978-3-319-11038-7_2
4. Y. Huang, X. Zhang, R. Zhao, H. Mao, Y. Yan, and X. Pang, Antibacterial Efficacy, Corrosion Resistance, and Cytotoxicity Studies of Copper-Substituted Carbonated Hydroxyapatite Coating on Titanium Substrate, *J. Mater. Sci.*, 2015, **50**, p 1688-1700. https://doi.org/10.1007/s10853-014-8730-1
5. L.C. Zhang and L.Y. Chen, A Review on Biomedical Titanium Alloys: Recent Progress and Prospect, *Adv. Eng. Mater.*, 2019, **21**, p 1801215. https://doi.org/10.1002/adem.201801215
6. M. Kaur and K. Singh, Review on Titanium and Titanium Based Alloys as Biomaterials for Orthopaedic Applications, *Mater. Sci. Eng. C*, 2019, **102**, p 844-862. https://doi.org/10.1016/j.msec.2019.04.064
7. M.A. Hussein, N.K. Ankah, A.M. Kumar, M.A. Azeem, S. Saravanan, A.A. Sorour, and N. Al Aqeeli, Mechanical, Biocorrosion, and Antibacterial Properties of Nanocrystalline TiN Coating for Orthopedic Applications, *Ceram. Int.*, 2020, **46**, p 18573-18583. https://doi.org/10.1016/j.ceramint.2020.04.164
8. S. Piscanec, L.C. Ciacchi, E. Vesselli, G. Comelli, O. Sbaizero, S. Meriani, and A. De Vita, Bioactivity of TiN-Coated Titanium Implants, *Acta Mater.*, 2004, **52**, p 1237-1245. https://doi.org/10.1016/j.actamat.2003.11.020
9. J. Zuo, Y. Xie, J. Zhang, Q. Wei, B. Zhou, J. Luo, Y. Wang, Z.M. Yu, and Z.G. Tang, TiN Coated Stainless Steel Bracket: Tribological, Corrosion Resistance, Biocompatibility and Mechanical Performance, *Surf. Coat. Technol.*, 2015, **277**, p 227-233. https://doi.org/10.1016/j.surfcoat.2015.07.009
10. A. Kozlovskiy, I. Shlimas, K. Dukenbayev, and M. Zdorovets, Structure and Corrosion Properties of Thin TiO_2 Films Obtained by Magnetron Sputtering, *Vacuum*, 2019, **164**, p 224-232. https://doi.org/10.1016/j.vacuum.2019.03.026
11. H. Sugisawa, H. Kitaura, K. Ueda, K. Kimura, M. Ishida, Y. Ochi, A. Kishikawa, S. Ogawa, and T.T. Yamamoto, Corrosion Resistance and Mechanical Properties of Titanium Nitride Plating on Orthodontic Wires, *Dent. Mater. J.*, 2018, **37**(2), p 286-292. https://doi.org/10.4012/dmj.2016-348
12. Z. Wang and Q.Z. Zhao, Friction Reduction of Steel by Laser-Induced Periodic Surface Nanostructures with Atomic Layer Deposited TiO_2 Coating, *Surf. Coat. Technol.*, 2018, **344**, p 269-275. https://doi.org/10.1016/j.surfcoat.2018.03.036
13. M. Łępicka, M.G. Dahlke, D. Pieniak, K. Pasierbiewicz, K. Kryńska, and A. Niewczas, Tribological Performance of Titanium Nitride Coatings: A Comparative Study on TiN-Coated Stainless Steel and Titanium Alloy, *Wear*, 2019, **422**, p 68-80. https://doi.org/10.1016/j.wear.2019.01.029
14. L. Visai, L. De Nardo, C. Punta, L. Melone, A. Cigada, M. Imbriani, and C.R. Arciola, Titanium Oxide Antibacterial Surfaces in Biomedical Devices, *Int. J. Artif. Organs*, 2011, **34**(9), p 929-946. https://doi.org/10.5301/ijao.5000050. (**PMID: 22094576**)
15. D. Wiedmer, C. Cui, F. Weber, F. Petersen, and H. Tiainen,Antibacterial Surface Coating for Bone Scaffolds Based on the Dark Catalytic Effect of Titanium Dioxide, *ACS Appl. Mater. Interfaces*, 2018, **10**(42), p 35784-35793. https://doi.org/10.1021/acsami.8b12623
16. X. Zhang, Y. Wu, Y. Lv, Y. Yu, and Z. Dong, Formation Mechanism, Corrosion Behaviour and Biological Property of Hydroxyapatite/TiO_2 Coatings Fabricated by Plasma Electrolytic Oxidation, *Surf. Coat. Technol.*, 2020, **386**, p 125483. https://doi.org/10.1016/j.surfcoat.2020.125483
17. E.M. Saeed, N.M. Dawood, and S.F. Hasan,Improvement Corrosion Resistance of Ni-Ti Alloy by TiO2 Coating and Hydroxyaptite/TiO2 Composite Coating Using Micro Arc Oxidation Process, *Mater. Today Proc.*, 2021, **42**(5), p 2789-2796. https://doi.org/10.1016/j.matpr.2020.12.723
18. R. Bahi, C. Nouveau, N.E. Beliardouh, C.E. Ramoul, S. Meddah, and O. Ghelloudj, Surface Performances of Ti-6Al-4V Substrates Coated PVD Multilayered Films in Biological Environments, *Surf. Coat. Technol.*, 2020, **385**, p 125412. https://doi.org/10.1016/j.surfcoat.2020.125412
19. E. Győri, I. Fábián, and I. Lázár,Effect of the Chemical Composition of Simulated Body Fluids on Aerogel-Based Bioactive Composites, *J. Compos. Sci.*, 2017, **1**(2), p 15-27. https://doi.org/10.3390/jcs1020015
20. C.C. Chien, K.T. Liu, J.G. Duh, K.W. Chang, and K.H. Chung,Effect of Nitride Film Coatings on Cell Compatibility, *Dent. Mater. J.*, 2008, **24**(7), p 986-993. https://doi.org/10.1016/j.dental.2007.11.020
21. M. Atapour, V. Rajaei, S. Trasatti, M.P. Casaletto, and G.L. Chiarello, Thin Niobium and Niobium Nitride PVD Coatings on AISI 304 Stainless Steel as Bipolar Plates for PEMFCs, *Coatings*, 2020, **10**(9), p 889-916. https://doi.org/10.3390/coatings10090889
22. V. Vishwakarma, G.S. Kaliaraj, D. Ramachandran, and A. Ramadoss, Bacterial Adhesion and Hemocompatibility Behavior of TiN, TiO_2 Single and TiN/tio$_2$ Multilayer Coated 316L SS for Bioimplants, *J. Biomimet. Biomater. Biomed. Eng.*, 2015, **25**, p 73-82. https://doi.org/10.4028/www.scientific.net/jbbbe.25.73
23. J.D.C. Tardelli, V.S. Bagnato, and A.C.D. Reis, Bacterial Adhesion Strength on Titanium Surfaces Quantified by Atomic Force Microscopy: A Systematic Review, *Antibiotics*, 2023, **12**(6), p 994-1010. https://doi.org/10.3390/antibiotics12060994
24. A.O. Ijaola, E.A. Bamidele, C.J. Akisin, I.T. Bello, A.T. Oyatobo, A. Abdulkareem, P.K. Farayibi, and E. Asmatulu,Wettability Transition for Laser Textured Surfaces: A Comprehensive Review, *Surf. Interfaces*, 2020, **21**, p 100802. https://doi.org/10.1016/j.surfin.2020.100802
25. P.G. Grützmacher, S.V. Jalikop, C. Gachot, and A. Rosenkranz, Thermocapillary Lubricant Migration on Textured Surfaces-A Review of Theoretical and Experimental Insights, *Surf. Topogr. Metrol. Prop.*, 2021, **9**(1), p 013001. https://doi.org/10.1088/2051-672X/abd07c
26. R. Shah, B. Gashi, S. Hoque, M. Maria, and A. Rosenkranz, Enhancing Mechanical and Biomedical Properties of Prostheses—Surface and Material Design, *Surf. Interfaces*, 2021, **27**, p 101498. https://doi.org/10.1016/j.surfin.2021.101498
27. V. Prakash, N. Priyadarshni, D. Aloc-Kumar, and S. Chattopadhyay, Fabrication of Hydrophobic Surface on Ti6Al4V by WEDM Process

for Surgical Instruments and Bioimplants, *Int. J. Adv. Manuf. Technol.*, 2022, **118**, p 1111-1123. https://doi.org/10.1007/s00170-021-07857-y
28. K. Sarkar, P. Jaipan, J. Choi, T. Haywood, D. Tran, N.R. Mucha, and S. Yarmolenko, Enhancement in Corrosion Resistance and Vibration Damping Performance in Titanium by Titanium Nitride Coating, *SN Appl. Sci.*, 2020, **2**, p 949-963. https://doi.org/10.1007/s42452-020-2777-1
29. M. Aslan Çakır, T. Yetim, A.F. Yetim, and A. Çelik, Superamphiphobic TiO_2 Film by Sol-Gel Dip Coating Method on Commercial Pure Titanium, *J. Mater. Eng. Perform.*, 2023 https://doi.org/10.1007/s11665-023-08049-3
30. H. Tekdir, T. Yetim, and A.F. Yetim, Corrosion Properties of Ceramic-Based TiO_2 Films on Plasma Oxidized Ti6Al4V/316L Layered Implant Structured Manufactured by Selective Laser Melting, *J. Bionic. Eng.*, 2021, **18**, p 944-957. https://doi.org/10.1007/s42235-021-0055-6
31. T. Rajabi, M. Atapour, H. Elmkhah, and S.M. Nahvi, Nanometric CrN/CrAlN and CrN/ZrN Multilayer Physical Vapor Deposited Coatings on 316L Stainless Steel as Bipolar Plate for Proton Exchange ,Membrane Fuel Cells, *Thin Solid Films*, 2022, **753**, p 139288. https://doi.org/10.1016/j.tsf.2022.139288
32. S.W.K. Kweh, K.A. Khor, and P. Cheang, Plasma-Sprayed Hydroxyapatite (HA) Coatings with Flame-Spheroidized Feedstock: Microstructure and Mechanical Properties, *Biomaterials*, 2000, **21**(12), p 1223-1234. https://doi.org/10.1016/S0142-9612(99)00275-6
33. L. Muller and F.A. Muller, Preparation of SBF with Different HCO^{-3} Content and its Influence on the Composition of Biomimetic Apatites, *Acta Biomater.*, 2006, **2**(2), p 181-189. https://doi.org/10.1016/j.actbio.2005.11.001
34. J. Kunze, L. Müller, J.M. Macak, P. Greil, P. Schmuki, and F.A. Muller, TiTime-Dependent Growth of Biomimetic Apatite on Anodic TiO_2 Nanotubes, *Electrochim. Acta*, 2008, **53**(23), p 6995-7003. https://doi.org/10.1016/j.electacta.2008.01.027
35. H.C. Hsu, S.C. Wu, S.K. Hsu, Y.C. Chang, and W.F. Ho, Fabrication of Nanotube Arrays on Commercially Pure Titanium and Their Apatite-Forming Ability in a Simulated Body Fluid, *Mater. Charact.*, 2015, **100**, p 170-177. https://doi.org/10.1016/j.matchar.2014.12.023
36. M. Svetina, L.C. Ciacchi, O. Sbaizero, S. Meriani, and A. De Vita, Deposition of Calcium Ions on Rutile (110): A First-Principles Investigation, *Acta Mater.*, 2001, **49**(12), p 2169-2177. https://doi.org/10.1016/S1359-6454(01)00136-7
37. A. Roguska, M. Pisarek, A. Belcarz, L. Marcon, M. Holdynski, M. Andrzejczuk, and M. Janik-Czachor, Improvement of the Bio-Functional Properties of TiO_2 Nanotubes, *Appl. Surf. Sci.*, 2016, **388**, p 775-785. https://doi.org/10.1016/j.apsusc.2016.03.128
38. H.R. Bakhsheshi-Rad, E. Hamzah, M.R. Abdul-Kadir, S.N. Saud, M. Kasiri-Asgarani, and R. Ebrahimi-Kahrizsangi,The Mechanical Properties and Corrosion Behavior of Double-Layered Nano Hydroxyapatite-Polymer Coating on Mg-Ca Alloy, *J. Mater. Eng. Perform*, 2015, **24**, p 4010-4021. https://doi.org/10.1007/s11665-015-1661-4
39. N.K. Nga, N.T.T. Chau, and P.H. Viet,Facile Synthesis of Hydroxyapatite Nanoparticles Mimicking Biological Apatite from Eggshells for Bone-Tissue Engineering, *Colloids Surf. B Biointerfaces*, 2018, **172**, p 769-778. https://doi.org/10.1016/j.colsurfb.2018.09.039
40. R. Malhotra, B. Dhawan, B. Garg, V. Shankar, and T.C. Nag, A Comparison of Bacterial Adhesion and Biofilm Formation on Commonly Used Orthopaedic Metal Implant Materials: An in Vitro Study, *Indian J. Orthop.*, 2019, **53**, p 148-153. https://doi.org/10.4103/ortho.IJOrtho_66_18
41. B. Del Curto, M.F. Brunella, C. Giordano, M.P. Pedeferri, V. Valtulina, L. Visai, and A. Cigada,Decreased Bacterial Adhesion to Surface-Treated Titanium, *Int. J. Artif. Organs*, 2005, **28**(7), p 718-730. https://doi.org/10.1177/039139880502800711
42. I. Yoda, H. Koseki, M. Tomita, T. Shida, H. Horiuchi, H. Sakoda, and M. Osaki, Effect of Surface Roughness of Biomaterials on Staphylococcus Epidermidis Adhesion, *BMC Microbiol.*, 2014, **14**(1), p 1-7. https://doi.org/10.1186/s12866-014-0234-2
43. C. Lüdecke, M. Roth, W. Yu, U. Horn, J. Bossert, and K.D. Jandt, Nanorough Titanium Surfaces Reduce Adhesion of Escherichia Coli and Staphylococcus Aureus Via Nano Adhesion Points, *Colloids Surf. B Biointerfaces*, 2016, **145**, p 617-625. https://doi.org/10.1016/j.colsurfb.2016.05.049
44. Y. Wu, J.P. Zitelli, K.S. TenHuisen, X. Yu, and M.R. Libera,Differential Response of Staphylococci and Osteoblasts to Varying Titanium Surface Roughness, *Biomaterials*, 2011, **32**, p 951-960. https://doi.org/10.1016/j.biomaterials.2010.10.001
45. P.A. Slullitel, M.A. Buttaro, G. Greco, J.I. Oñativia, M.L. Sánchez, S. Mc Loughlin, C. García-Ávila, F. Comba, G. Zanotti, and F. Piccaluga, No Lower Bacterial Adhesion for Ceramics Compared to Other Biomaterials: An in Vitro Analysis, *Orthop. Traumatol. Sur.*, 2018, **104**(4), p 439-443. https://doi.org/10.1016/j.otsr.2018.03.003